

Structures in the Great Attractor Region

D. J. Radburn-Smith¹, J. R. Lucey¹, P. A. Woudt², R. C. Kraan-Korteweg²,
F. G. Watson³

¹*Department of Physics, University of Durham, South Road, Durham DH1 3LE, UK*

²*Department of Astronomy, University of Cape Town, Rondebosch 7700, South Africa*

³*Anglo-Australian Observatory, Coonabarabran, NSW 2357, Australia*

1 August 2021

ABSTRACT

To further our understanding of the Great Attractor (GA), we have undertaken a redshift survey using the 2dF on the AAT. Clusters and filaments in the GA region were targeted with 25 separate pointings resulting in approximately 2600 new redshifts. Targets included poorly studied X-ray clusters from the CIZA catalogue as well as the Cen-Crux and PKS 1343-601 clusters, both of which lie close to the classic GA centre. For nine clusters in the region, we report velocity distributions as well as virial and projected mass estimates. The virial mass of CIZA J1324.7–5736, now identified as a separate structure from the Cen-Crux cluster, is found to be $\sim 3 \times 10^{14} M_{\odot}$, in good agreement with the X-ray inferred mass. In the PKS 1343-601 field, five redshifts are measured of which four are new. An analysis of redshifts from this survey, in combination with those from the literature, reveals the dominant structure in the GA region to be a large filament, which appears to extend from Abell S0639 ($l = 281^{\circ}$, $b = +11^{\circ}$) to ($l \sim 5^{\circ}$, $b \sim -50^{\circ}$), encompassing the Cen-Crux, CIZA J1324.7–5736, Norma and Pavo II clusters. Behind the Norma Cluster at $cz \sim 15000 \text{ km s}^{-1}$, the masses of four rich clusters are calculated. These clusters (Triangulum-Australis, Ara, CIZA J1514.6–4558 and CIZA J1410.4–4246) may contribute to a continued large-scale flow beyond the GA. The results of these observations will be incorporated into a subsequent analysis of the GA flow.

Key words: galaxies: clusters: general – galaxies: distances and redshifts – large-scale structure of Universe

1 INTRODUCTION

Peculiar velocities are vital probes of the large scale mass distribution in the local Universe that do not rely on the assumption that light traces mass. Early work by Lynden-Bell et al. (1988) made the unexpected discovery of a 600 km s^{-1} outflow towards Centaurus. This led to the idea of a large, extended mass overdensity, nicknamed the Great Attractor (GA), dominating the dynamics of the local Universe. Whilst many studies have confirmed the presence of the GA (e.g. Aaronson et al. 1989), the precise mass, position and extent of the overdensity remain uncertain. Lynden-Bell et al. (1988) originally located the GA at (l, b, cz) $\sim (307^{\circ}, +9^{\circ}, 4350 \pm 350 \text{ km s}^{-1})$ with a mass of $5.4 \times 10^{16} M_{\odot}$. However a subsequent study by Kolatt, Dekel & Lahav (1995) placed the GA peak at ($320^{\circ}, 0^{\circ}, 4000 \text{ km s}^{-1}$), whilst Tonry et al. (2000) favoured an even closer locale at ($289^{\circ}, +22^{\circ}, 3200 \pm 260 \text{ km s}^{-1}$) and a mass approximately six times smaller ($\sim 8 \times 10^{15} M_{\odot}$). As the GA lies in the Zone of Avoidance (ZoA), foreground ex-

inction and high stellar contamination have hampered studies of the underlying galaxy distribution. Recently, however, several key results have emerged.

The Norma cluster (Abell 3627), located at ($325^{\circ}, -7^{\circ}, 4848 \text{ km s}^{-1}$), is now recognised to be comparable in mass, richness and size to the Coma cluster (Kraan-Korteweg et al. 1996). Lying $\sim 9^{\circ}$ from the Kolatt et al. (1995) location of the GA, the cluster has been identified as a likely candidate for the ‘core’ of the overdensity (Woudt 1998). Furthermore, it has been suggested that the GA is a ‘Great Wall’ like structure that extends from low galactic latitudes, encompassing the Pavo II ($332^{\circ}, -24^{\circ}, 4200 \text{ km s}^{-1}$, Lucey & Carter 1988) and Norma clusters before bending over and continuing towards $l \sim 290^{\circ}$ (Kraan-Korteweg & Woudt 1994; Woudt et al. 1997, 2004). This connection has been labelled the Norma supercluster (Fairall et al. 1998) and constitutes the major structure in the GA region (defined here as $280^{\circ} < l < 360^{\circ}$, $-45^{\circ} < b < +30^{\circ}$, $3000 < cz < 7000 \text{ km s}^{-1}$).

The richness of such connective structures in the re-

gion have been highlighted by recent blind HI surveys in the southern sky (Kraan-Korteweg et al. 2005b; Koribalski 2005; Henning et al. 2005). Because the ZoA is effectively transparent to 21 cm radiation, these surveys are able to trace the full extent of the local large-scale filaments as they pass through the plane. Notably, between galactic latitudes of -5° and $+5^\circ$, Henning et al. (2005) find evidence for an extension of the Norma supercluster at $cz \sim 5000 \text{ km s}^{-1}$, running from $b = 300^\circ$ to 340° .

The X-ray selected ‘Clusters In the Zone of Avoidance’ (CIZA) project has revealed several new X-ray clusters at low galactic latitudes (Ebeling, Mullis & Tully 2002; Kocevski et al. 2005). In the GA region, this survey has identified CIZA J1324.7–5736 as another potentially sizeable contributor to the GA’s mass. Lying at $(307^\circ, +5^\circ, 5700 \text{ km s}^{-1})$ this cluster has been associated with the overdensity previously identified as the Cen-Crux cluster (Woudt 1998). X-ray measurements suggest that the structure is comparable in mass to the Norma cluster (Mullis et al. 2005).

Another important cluster in the GA region may exist around PKS 1343-601, an extremely strong radio source lying in the ZoA (Kraan-Korteweg & Woudt 1999). The host galaxy is a large E0 (Laustsen, Schuster & West 1977; West & Tarengi 1989) located at $\sim (310^\circ, +2^\circ, 3900 \text{ km s}^{-1})$. Despite the lack of an associated X-ray source (Ebeling et al. 2002), recent near-infrared surveys are consistent with the presence of an intermediate mass cluster centred on the radio source (Kraan-Korteweg et al. 2005a; Schröder et al. 2005; Nagayama et al. 2004).

Attempts to analyse the extent and mass of the GA from peculiar velocity measurements have remained inconclusive. To date, no clear sign of any backside infall has been detected (Mathewson, Ford & Buchhorn 1992; Hudson 1994). This has been attributed to a continuing high amplitude flow, possibly due to the gravitational pull of the Shapley supercluster (SSC, Scaramella et al. 1989; Raychaudhury 1989; Branchini et al. 1999; Hudson et al. 2004). Centred on Abell 3558 ($312^\circ, 31^\circ, 14500 \text{ km s}^{-1}$), the SSC is an extremely rich concentration of galaxies. Dynamical analysis by Reisenegger et al. (2000) of the collapsing core of the SSC, indicates that the mass contained within the central $8 h^{-1} \text{ Mpc}$ is between 2×10^{15} and $1.3 \times 10^{16} h^{-1} M_\odot$. However different estimates of the SSC’s mass, derived from various surveys of the region, vary significantly due to differing assessments of the extent and geometry of the structure (see Bardelli et al. 2000). Furthermore, recent analysis suggests that intercluster galaxies may compose up to two thirds of the SSC’s mass, thus severely biasing previous estimates based solely on summed cluster masses (Proust et al. 2005). Accounting for all the galaxies in their 285 deg^2 survey of the SSC, Proust et al. (2005) estimate an enclosed mass of $5 \times 10^{16} h^{-1} M_\odot$.

This uncertainty in the relative masses of the GA and the SSC has led to much dispute over the predicted source of the bulk flow observed in the local Universe and hence the source of the Local Group’s (LG) own motion. Ettori et al. (1997) and Rowan-Robinson et al. (2000) estimated that the SSC was only responsible for approximately 5 per cent of the LG’s motion. However, Bardelli et al. (2000) placed the contribution closer to ~ 15 per cent whilst others have advocated values of up to 50 per cent (e.g.

Smith et al. 2000; Lucey, Radburn-Smith & Hudson 2005; Kocevski et al. 2005).

In order to further understand the nature of the GA, and hence the role it plays in the LG’s motion, we have undertaken a redshift survey with the Two-degree Field multi-fibre spectrograph (2dF). Targets include five of the CIZA clusters (including the Cen-Crux cluster), the PKS 1343–601 region and overdensities located along the proposed filamentary structures. We describe these observations and present the redshift measurements in Section 2 where we also discuss errors and completeness. Analysis of the identified structures are presented in Section 3 and in Section 4 we summarise our findings.

2 OBSERVATIONS AND DATA REDUCTION

Observations were carried out in two runs on the 3.9m Anglo-Australian Telescope (AAT). The 2dF was configured using the same set up as that used for the 2dF Galaxy Redshift Survey (2dFGRS Colless et al. 2001). This included using the 300B gratings with the $1024 \times 1024 \text{ } 24 \mu\text{m}$ pixels on the Tektronix CCDs, resulting in a dispersion of $178.8 \text{ \AA mm}^{-1}$ or $4.3 \text{ \AA pixel}^{-1}$. At the centre of the chip, the FWHM of the focus is about 2 pixels, hence the typical spectral resolution is 9 \AA . Additionally, a central wavelength of 5800 \AA was chosen to cover a range of about $3650\text{--}8050 \text{ \AA}$. Seeing over the course of the two runs was $\sim 1\text{--}1.5 \text{ arcsec}$.

In total, we observed 25 separate fields as listed in Table 1. A repeat observation of one field was also taken in order to assess systematics. Field centres were chosen to maximise the number of targeted galaxies, whilst fully encompassing known clusters and noticeable overdensities. Target galaxies were taken from the Two Micron All Sky Survey Extended Source Catalogue (2MASS XSC, Jarrett et al. 2000) and the NASA Extragalactic Database (NED). Additional targets in the Cen-Crux and PKS 1343–601 fields were identified using J , H and K_s observations taken with the 1.4 m InfraRed Survey Facility (IRSF, Nagayama et al. 2004, 2005) and I-band images from the Wide Field imager (WFI) at the ESO 2.2m telescope at La Silla (Kraan-Korteweg et al. 2005a). Suitable guide stars were selected from the Tycho 2 catalogue (Høg et al. 2000). 2MASS positions were used for both targets and guide stars, with counterparts identified from the 2MASS Point Source Catalogue (Cutri et al. 2003) for sources with no equivalent 2MASS XSC position.

After acquiring each target field, a flat field and an arc exposure, using copper-argon and copper-helium lamps, were taken for fibre identification and wavelength calibration. Three 900 s exposures of the fields yielded signal to noise ratios of $\sim 15\text{--}30$. However, seven 900 s exposures of targets in the PKS 1343–601 field achieved an average S/N ratio of only ~ 5 due to high galactic extinction ($A_B \sim 10$).

The data was reduced using the 2DFDR automatic data reduction program as described in Colless et al. (2001). The default settings were used with the exception of the use of sky flux methods for fibre throughput calibration, as no off-sky measurements were taken. Once reduced, redshifts were measured using the RUNZ program developed for the 2dFGRS (also described in Colless et al. 2001). This program uses the Tonry & Davis (1979) technique to cross correlate nine templates with the observed spectra in order to obtain

Table 1. Summary of 2dF observations. The (l, b) coordinates for each targeted field are listed. These are not necessarily identical to the coordinates of cluster centres, as small adjustments were made to maximise the number of galaxies available to fibres in each field.

Field No.	Target	l	b	Exposure length (s)	UT Date	No. Redshifts
1	Cen-Crux/CIZA J1324.7–5736 – 1	307.4	4.9	3×900	2004 Feb 29	46
2	Cen-Crux/CIZA J1324.7–5736 – 2	305.4	5.1	3×900	2004 Feb 29	51
3	Cen-Crux/CIZA J1324.7–5736 – 3	305.1	7.1	3×900	2004 Feb 29	40
4	Cen-Crux/CIZA J1324.7–5736 – 4	304.6	9.4	3×900	2005 Jun 9	87
5	PKS 1343-601	309.7	2.3	7×900	2004 Feb 29	5
6	Abell S0639	281.3	10.7	3×1200	2004 Feb 29	174
7	Triangulum-Australis/CIZA J1638.2–6420	324.7	–11.7	3×900	2005 Jun 8	252
8	Ara/CIZA J1653.0–5943	329.2	–9.8	3×900	2005 Jun 8	179
9	Cluster 1	314.3	13.9	3×900	2005 Jun 8	225
10	CIZA J1514.6–4558	327.3	10.2	3×1200	2005 Jun 7	226
11	CIZA J1410.4–4246	317.9	17.8	3×900	2005 Jun 8	182
12	Filament 1	296.3	9.1	4×900 & 1×712	2005 Jun 8	135
13	Hydra-Antlia Extension 1	281.8	–6.2	3×900	2005 Jun 9	91
14	Hydra-Antlia Extension 2	280.6	–7.8	3×900	2005 Jun 9	126
15	Filament 2	300.4	9.0	3×900	2005 Jun 9	83
16	Filament 3	299.8	6.9	3×900	2005 Jun 9	50
17	Filament 4	312.5	5.0	4×900	2005 Jun 8	60
18	Filament 5	316.6	8.1	3×900	2005 Jun 9	70
19	Filament 6	312.9	9.0	3×900	2005 Jun 9	101
20	Filament 7	312.6	12.4	3×900	2005 Jun 8	111
21	Filament 8	351.0	–22.6	3×900	2005 Jun 8	146
22	Filament 9	355.3	–33.0	2×900	2005 Jun 8	175
23	Filament 10/RXC J1840.6-7709	317.7	–25.5	3×900	2005 Jun 9	156
24	Filament 11/CIZA J1407.8–5100	315.0	10.2	3×900	2005 Jun 9	91
25	Cluster 2	322.3	13.6	3×900	2005 Jun 9	155
26	Ara/CIZA J1653.0–5943 – repeat	329.2	–9.8	4×900	2005 Jun 9	169

the best absorption redshift. Where available, the program also determines emission redshifts by matching O II, H β , O III, H α , N II and S II features.

2.1 Redshifts

A total of 3053 redshifts were measured, 2603 of which are not listed in NED (as of 2006 February 15). Table 2 lists a representative sample of the complete table which can be found online¹.

Emission line redshifts are reported for approximately 32 per cent of the sample, whilst absorption line based cross correlation redshifts are available for ~ 96 per cent. For the ~ 27 per cent identified through both absorption and emission features, the absorption redshift is found to be larger on average by ~ 58 km s^{–1}. This difference, which is usually attributed to gas outflows, is consistent with offsets found in other galaxy surveys (e.g. Cappi et al. 1998).

In order to assess the combined reliability of the observations and data reduction, a repeat observation of one

Table 2. A representative sample of the full table published online. Both heliocentric absorption and emission redshifts are listed where measured. Column 1 lists the galaxy identification. The 2MASS XSC name is given first and then the equivalent NED identification². J2000 equatorial coordinates are listed as either part of the name of the target or after the colon in the first column. The 2MASS J -band magnitude (j_{m_ext}), extrapolated from a fit to the radial surface brightness profile, is listed in column 2 where available. Columns 3 and 4 list the heliocentric velocities (cz km s^{–1}) identified through absorption and emission features respectively. As discussed below, the uncertainty on each measurement is ± 85 km s^{–1}.

Name	J_{Ext}	cz_{ab}	cz_{em}
Field: 1 (RA:201.17° Dec:-57.68° l:307.78° b:4.90°)			
2MASX J13184671-5804502	13.00		14774
2MASX J13190643-5744311	12.38	5552	5507
2MASX J13200919-5725561	12.15	4578	
2MASX J13203723-5752421	11.57	5469	
2MASX J13211580-5827564	12.71	6155	
2MASX J13212199-5718084	14.11	6949	6835
2MASX J13220594-5728001	12.15	5706	
2MASX J13230235-5732041	12.15	5204	
2MASX J13230489-5740301	12.38	5841	5798
2MASX J13231390-5709190	12.28	5763	
2MASX J13232993-5744020	13.22	6068	
NNSW71:J13233545-5747205			32701
2MASX J13233881-5807500	12.19	5444	
2MASX J13234325-5731460	13.20	6433	
2MASX J13234503-5742550	12.65	4426	
2MASX J13235263-5723200	12.29	5967	5870
...

¹ The full table will be published online in the electronic edition of this journal and on the CDS

² As of March 2006, seven galaxies are contained in neither the NED or 2MASS XSC catalogues: Two galaxies identified with the prefix KKOWA were found from ESO 2.2m WFI I -band observations around PKS 1343-601 (Kraan-Korteweg et al. 2005a), two galaxies, labelled NNSW, are taken from NIR IRSF observations around Cen-Crux (Nagayama et al. 2005) and a further three galaxies, labelled DJRS, are new identifications from searches of DSS images.

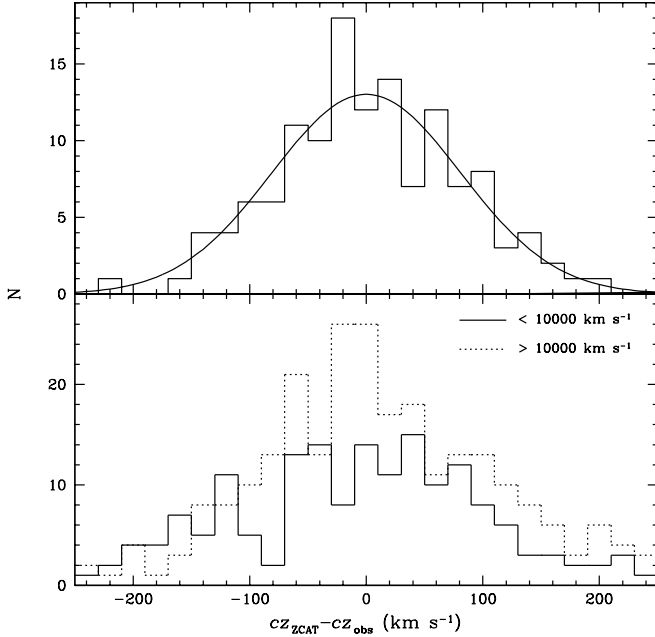


Figure 1. The top panel shows the difference between repeat observations of the same field. A Gaussian fit to the dispersion yields a value of $\sigma = 114 \text{ km s}^{-1}$, corresponding to a single measurement rms uncertainty of 81 km s^{-1} . The bottom panel plots the difference between coincident measurements from the ZCAT catalogue. Histograms are plotted separately for data within 10000 km s^{-1} and for data beyond as coincident measurements primarily fall into two distinct velocity ranges around 6000 km s^{-1} and 15000 km s^{-1} . The mean offset of the points is $+2 \text{ km s}^{-1}$ and the scatter is consistent with an error of 89 km s^{-1} on our data points.

field (Ara/CIZA J1653.0–5943) was made. The difference between these measurements (shown in the top panel of Fig. 1) implies an rms uncertainty on a single measurement of 81 km s^{-1} .

The lower panel of Fig. 1 shows the residual differences between our data and those from ZCAT (Huchra et al. 1992, , 2005 November 27 edition). Coincident galaxies between the catalogues were found through name matching and searching for separations of less than 4 arcsec. For the resulting 433 galaxies, a negligible offset of only $+2 \text{ km s}^{-1}$ is found. A value of $\chi^2_\nu \sim 1$ is achieved by adopting an uncertainty of 89 km s^{-1} on our values and using the quoted ZCAT errors, which in the absence of multiple measurements are taken directly from the original source. At $cz \sim 6500 \text{ km s}^{-1}$, the comparison exhibits an excess of negative values (i.e. ZCAT values significantly lower than the redshifts reported here). This can be attributed to the inclusion in ZCAT of redshifts for galaxies in Abell S0639 as measured by Stein (1996). These measurements are offset from the rest of the ZCAT catalogue by $\sim -140 \text{ km s}^{-1}$, causing the enhancement around this value in the residual histogram that represents comparisons within 10000 km s^{-1} .

Comparison of the 221 galaxies in common with the 6dF Galaxy Survey (6dFGS 2DR, Jones et al. 2005) indicates an error of 94 km s^{-1} with a mean offset of $+3 \text{ km s}^{-1}$. Whilst analysis of the 96 galaxies also observed by Woudt et al.

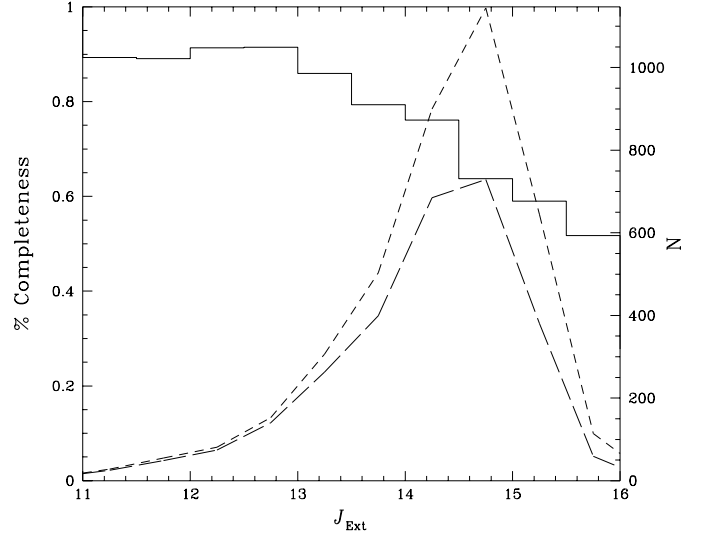


Figure 2. The completeness of targeted galaxies. The solid histogram indicates the percentage of targeted galaxies in each 0.5 mag bin for which a reliable redshift was discernible. The short and long dashed lines show respectively the total number of galaxies targeted and the number actually recorded in each corresponding bin.

(2004) yields an 89 km s^{-1} uncertainty and $+19 \text{ km s}^{-1}$ offset. Hence, as with the 2DFGRS (Colless et al. 2001), we adopt an underlying random error of 85 km s^{-1} on all our measurements.

The completeness of the observed 2MASS galaxies as a function of the extrapolated J -band magnitude is shown in Fig. 2. The vast majority of targeted galaxies lie in the range $12 < J_{\text{Ext}} < 16 \text{ mag}$. Typically 10 per cent of these yield no reliable redshift due to dominant stellar contamination. Hence this survey has good completeness to $J = 13 \text{ mag}$, after which a steady decline is observed down to an effective completeness of ~ 60 per cent for the faintest galaxies at $J > 16 \text{ mag}$. To illustrate the depth of the survey we calculate the characteristic magnitude at the distance of the GA and the SSC. By fitting a Schechter function to the combined 2dFGRS/2MASS infrared catalogue, Cole et al. (2001) find a magnitude corresponding to the characteristic luminosity L^* of $M_J^* - 5 \log h = -22.36 \pm 0.02$. Using this value we find an apparent magnitude of $J \sim 11 \text{ mag}$ at the GA ($cz \sim 4500 \text{ km s}^{-1}$) and $\sim 13.5 \text{ mag}$ at the SSC ($cz \sim 14500 \text{ km s}^{-1}$). Around the Norma cluster and the SSC, extinction is typically $A_J \sim 0.17$ and 0.05 mag respectively.

3 LARGE-SCALE STRUCTURES IN THE GA/SSC DIRECTION

The redshift distribution for each of the surveyed fields is shown in Fig. 3. Immediately obvious are the large overdensities in fields 1,2 & 6–11 corresponding to the targeted clusters. The structures in which these clusters are embedded are also apparent in many of the fields as features at

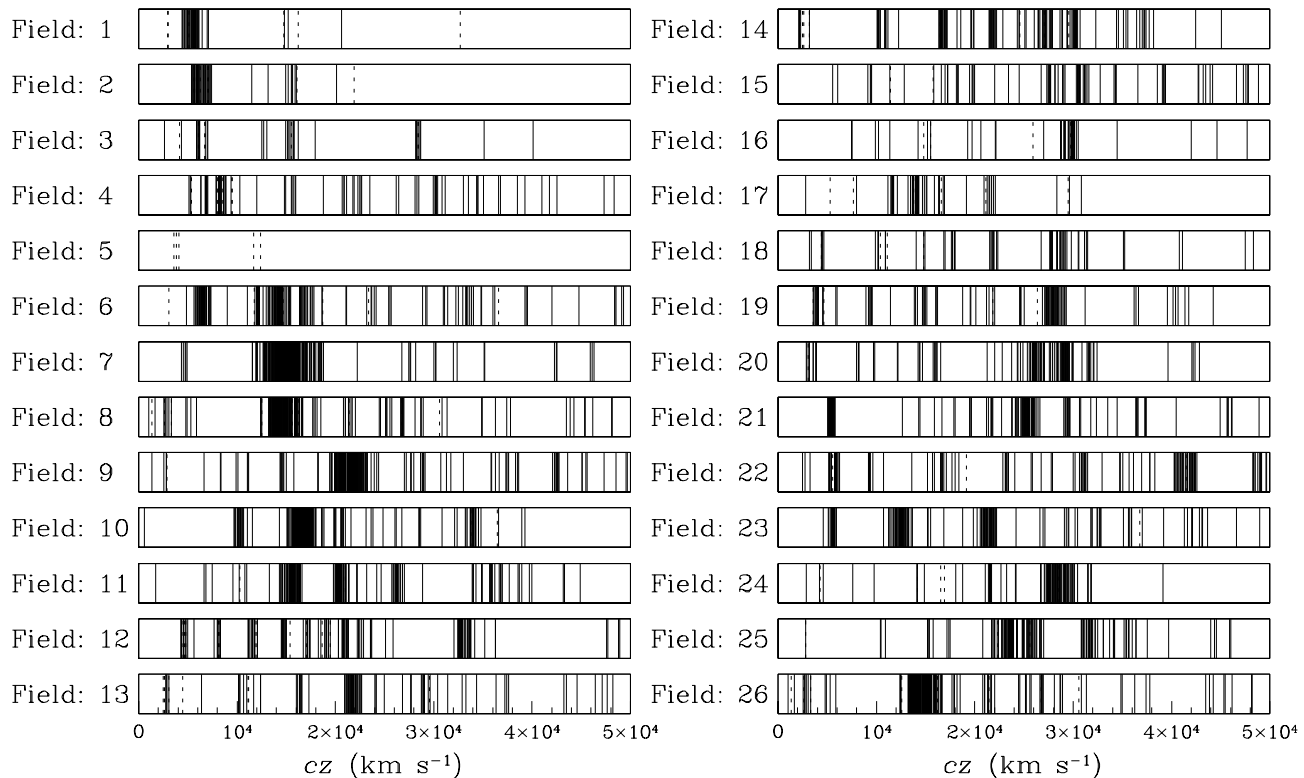


Figure 3. Distribution of radial velocities in each of the 26 targeted fields listed in Table 1. Dashed lines refer to redshifts derived through observed emission lines, whilst solid lines indicate measurements made via cross-correlation with template spectra. Note that field 26 is a repeat observation of field 8.

redshifts of around $2000\text{--}6000\text{ km s}^{-1}$ and $\sim 15000\text{ km s}^{-1}$, corresponding to the GA and SSC respectively.

3.1 Review of large scale structures

The number of redshifts known in the GA and SSC region have greatly increased with the recent completion of surveys such as FLASH (Kaldare et al. 2003), 6dFGS, the SSC study of Proust et al. (2005) and the ‘extragalactic large-scale structures behind the southern Milky Way’ project (Kraan-Korteweg & Woudt 1994; Fairall, Woudt & Kraan-Korteweg 1998; Woudt, Kraan-Korteweg & Fairall 1999; Woudt et al. 2004). Together with our measurements, we use these recent surveys to assess the large-scale structures traced by the galaxies in this important region. Fig. 4 plots the combined projected distribution of the redshifts. The first panel identifies the 2dF fields observed by this survey. The majority of the fields lie in regions outside the 6dFGS survey limit (i.e. $b < |10|^\circ$) and predominantly near 2MASS over-densities close to the classic GA centre. Abell clusters are identified in the last two panels, whilst the remaining panels present the data in successive redshift slices, which contain the following relevant structures:

$cz \leq 2000\text{ km s}^{-1}$: In this panel, a line of galaxies crossing the Galactic plane at $l=280^\circ$ and extending to the centre of the Virgo Cluster (off the panel at $l=280^\circ$,

$b=+74^\circ$) is clearly seen. These belong to the Virgo Supercluster, which encircles the entire sky and defines the Supergalactic Plane. The smaller Fornax Wall is also seen here face-on (Fairall 1998). It appears as a filament of galaxies running from the Fornax cluster ($237^\circ, -54^\circ$) and crossing the Galactic plane at $l=295^\circ$. The extension of these filaments through the ZoA is traced by the HI galaxies from surveys based on the HI Parkes All-Sky Survey (HIPASS, Barnes et al. 2001), most notably the HIPASS Bright Galaxy Catalogue (Koribalski et al. 2004) and the deep HIPASS catalogue (HICAT, Meyer et al. 2004).

$2000 < cz \leq 4000\text{ km s}^{-1}$: Immediately apparent in the third panel, is the Centaurus cluster (Abell 3526) lying at ($302^\circ, +22^\circ$). Extending down from this cluster and through the galactic plane is the Centaurus Wall. This wall crosses a large part of the southern sky and is one of the most prominent features in all-sky maps of galaxies within 6000 km s^{-1} (Fairall 1998). As we lie close to the plane of the Centaurus Wall, the structure is seen edge-on (Fairall 1998).

Almost perpendicular to the Centaurus Wall is the Hydra Wall (Fairall 1998). This is seen here as a filament of galaxies reaching out from the Centaurus cluster, through the Hydra ($270^\circ, +27^\circ$) and Antlia ($273^\circ, +19^\circ$) clusters before heading on to the Puppis cluster ($240^\circ, 0^\circ$, Lahav et al. 1993) and down towards ($210^\circ, -30^\circ$).

The Hydra-Antlia extension (Kraan-Korteweg & Woudt 1994) forms a third fila-

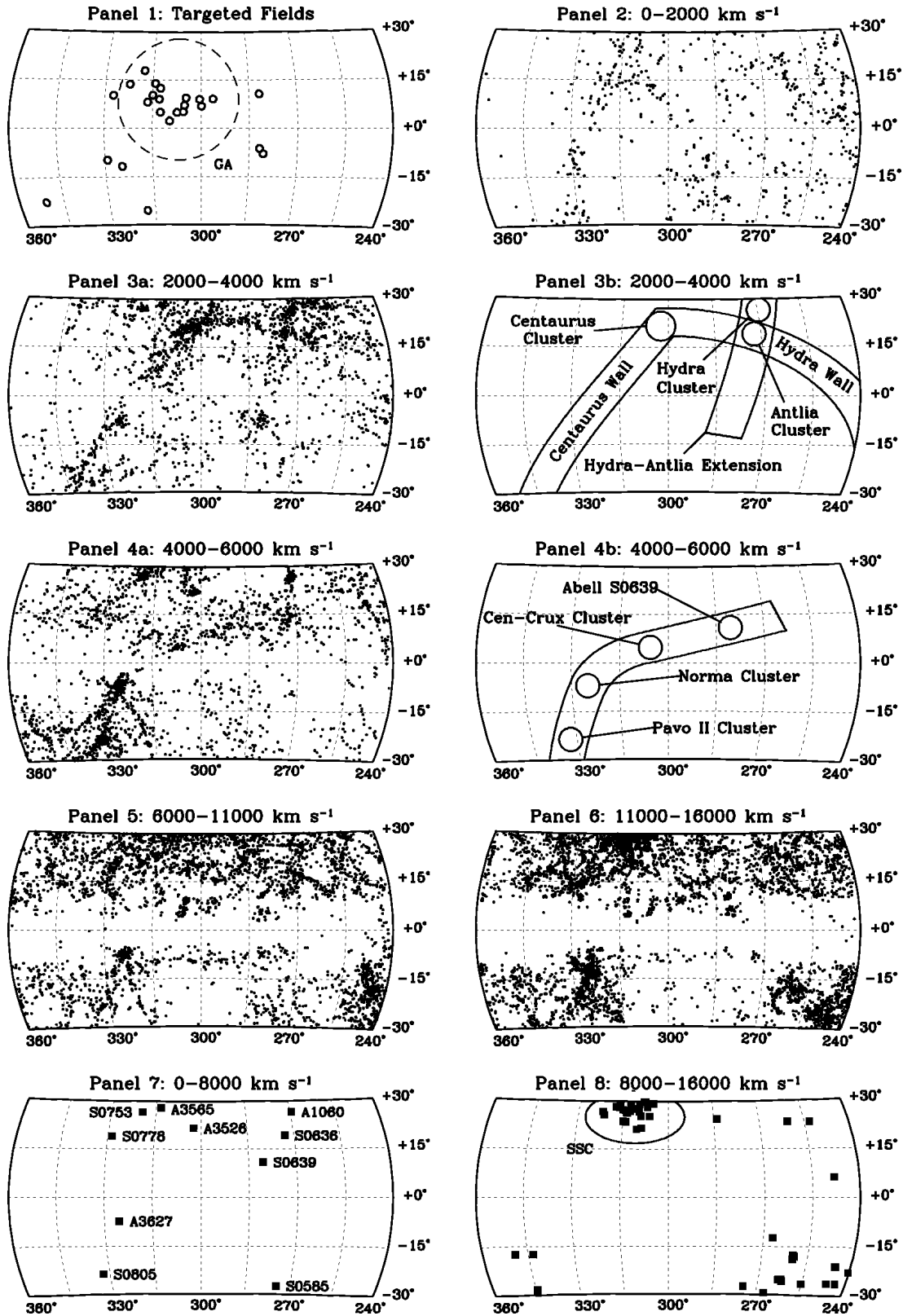


Figure 4. Aitoff projections of redshift slices containing galaxies in the range $240^\circ < l < 360^\circ$ and $-30^\circ < b < +30^\circ$ from this survey and the NED database (as of 2006 February 15). The projected circles in the first panel represent the actual size of each 2dF target field located in the region. The dashed circle represents the core radius used in the spherical GA model of Faber & Burstein (1988) centred on $(306^\circ, +9^\circ)$. Panels 3b and 4b illustrate the key features observed in the corresponding redshift slices. Abell clusters within 8000 km s^{-1} are labelled in Panel 7, whilst in panel 8, Abell clusters between 8000 and 16000 km s^{-1} are plotted and the clusters composing the SSC are indicated.

mentary structure in this slice. From the Hydra cluster, this feature passes through the Antlia cluster, crosses the Galactic plane at $b = 278^\circ$ and ends in a group of galaxies at $(280^\circ, -8^\circ)$. Kraan-Korteweg & Woudt (1994) suggested that an overdensity of galaxies, named the Vela overdensity and located at $(280^\circ, +6^\circ)$, formed part of the Hydra-Antlia extension. However subsequent observations of this group have revealed that it lies significantly behind the extension at $cz = 6000 \text{ km s}^{-1}$ (Kraan-Korteweg et al. 1995).

4000 < cz ≤ 6000 km s⁻¹: The fourth panel reveals the massive Norma cluster of galaxies lying at $(325^\circ, -7^\circ)$. Below this and connected by a trail of galaxies is the Pavo II cluster (Abell S0805, $l = 332^\circ$, $b = -24^\circ$). Additionally, two smaller filaments of galaxies are seen extending down from the Norma cluster to both lower and higher galactic longitudes.

A less pronounced linear feature is also observed in this panel. Continuing from the connection between the Pavo II and Norma clusters, the structure extends across the Galactic plane and on through CIZA J1324.7–5736 ($307^\circ, +5^\circ$) and the Cen-Crux ($305^\circ, +5^\circ$) cluster before ending at Abell S0639 ($281^\circ, +11^\circ$). Collectively, this structure is known as the ‘Norma supercluster’ (Woudt et al. 1997) and is discussed further in Section 3.3.

6000 < cz ≤ 11000 km s⁻¹: The Norma cluster ‘finger of God’ is still evident in this panel. The linear feature at $b = -10^\circ$ that extends from this overdensity towards lower galactic latitudes, is an artificial enhancement due to the survey limit ($b \lesssim -10^\circ$) of the combined southern Milky Way survey (Kraan-Korteweg et al. 1995; Fairall et al. 1998; Woudt et al. 1999). The Vela overdensity and continuation of the Cen-Crux structure are both seen as distinct groups at $(305^\circ, +6^\circ)$ and $(280^\circ, +6^\circ)$ respectively. Also present is the Ophiuchus cluster (Hasegawa et al. 2000; Wakamatsu et al. 2005) lying at the edge of the panel ($360^\circ, +9^\circ, 8500 \text{ km s}^{-1}$).

11000 < cz ≤ 16000 km s⁻¹: In the last panel, the massive concentration of clusters that constitute the SSC becomes apparent around $(314^\circ, +30^\circ)$. Also visible are the large Ara ($329^\circ, -10^\circ$) and Triangulum-Australis ($325^\circ, -12^\circ$) clusters (lying almost directly behind the Norma cluster), CIZA J1514.6–4558 at $(327^\circ, +10^\circ)$ and CIZA J1410.4–4246 at $(318^\circ, +18^\circ)$.

3.2 Clusters

Of great importance in studying the GA flow is an assessment of the relative masses of the rich clusters in the region. Notably, the CIZA survey has identified several new X-ray clusters in the GA direction. We targeted six of these sources, which together with noticeable overdensities in the 2MASS XSC, made up nine fields containing possible clusters.

To determine if these systems were indicative of relaxed clusters, their velocity dispersions, culled by an iterative 3σ clipping procedure about their median, were tested for gaussianity. With no prior on the mean or standard deviation, the Shapiro-Wilk W-statistic (Shapiro & Wilk 1965) is able to test the null hypothesis that data is indeed sampled from a normal distribution. We accept this hypothesis if the associated p-value, calculated via the analytical approach of Royston (1995), is greater than 0.05.

If the W-statistic for a sample indicates that the redshifts were taken from a normal distribution, the corresponding velocity dispersion was determined using a method that includes measurement errors on individual redshifts (Danese, de Zotti & di Tullio 1980). Uncertainties on the derived values were calculated by bootstrap resampling.

The masses of the corresponding systems were calculated using the classical virial mass estimator, defined by Heisler et al. (1985) as

$$M_{\text{vir}} = \frac{3\pi N}{2G} \frac{\sum_i (v_i - \bar{v})^2}{\sum_{i,j < i} R_{ij}^{-1}}$$

where

$$R_{ij} = |R_i - R_j|$$

is the projected galaxy separation. This virial method has been shown to be a reliable first order approximation to the mass of a dynamically relaxed system which is fully contained within the observed field (e.g. see Rines et al. 2003). The projected mass estimator for each cluster was also calculated:

$$M_{\text{proj}} = \frac{32}{N\pi G} \sum_i R_i (v_i - \bar{v})^2.$$

Errors on both mass estimates were again assigned by bootstrap resampling. With their sample of nine clusters in the CAIRNS project, Rines et al. (2003) find that the projected mass is only 1.18 ± 0.05 times greater than the estimated virial mass. Hence, given the expected errors on the dispersions, the two estimators should be consistent.

Table 3 lists the mean redshift, velocity dispersion, mass estimate, W-statistic and associated p-value for the best fit to each of the observed clusters. These fits are plotted with the corresponding velocity histograms in Fig. 5.

3.2.1 Cen-Crux/CIZA J1324.7–5736

Multi-object spectroscopy of the GA region revealed an overdensity of galaxies at $(305^\circ, +5^\circ, 6214 \text{ km s}^{-1})$, which was named the Cen-Crux cluster (Woudt 1998; Fairall et al. 1998; Woudt et al. 2004). Later, an associated X-ray cluster signature was detected by the CIZA survey at $(307^\circ, +5^\circ)$. Preliminary analysis of the X-ray source (CIZA J1324.7–5736) suggested that it was comparable in mass to the Norma cluster (Ebeling et al. 2002).

We have observed one field centred on the X-ray source and three further fields targeting the surrounding overdensities (see Fig. 6). Of the 223 identified redshifts in the targeted fields, 110 are within 7500 km s^{-1} . Two distinct structures are observed within these fields.

Ebeling et al. (2002) noted that the appearance of the X-ray emissions in the region and their association with the brightest cluster galaxy WKK2189 ($cz = 5585 \text{ km s}^{-1}$), were suggestive of a dynamically relaxed cluster. 40 of the observed galaxies are found to be associated with the X-ray source. Shown in the Field 1 histogram on the right hand side of Fig. 6, the velocity dispersion of these galaxies is $539 \pm 80 \text{ km s}^{-1}$ centred on $5570 \pm 92 \text{ km s}^{-1}$. The Shapiro-Wilk test on this distribution yields a p-value of 0.1176 and the estimated virial mass is $(3.5 \pm 1.0) \times 10^{14} h^{-1} M_\odot$. Hence the interpretation of a large relaxed cluster is supported here by the observed Gaussian velocity distribution.

Table 3. Parameters for the fits to the velocity distributions of the observed clusters as detailed in Section 3.2.

Cluster Name	\bar{v} km s ⁻¹	σ km s ⁻¹	M_{Virial} $h^{-1} M_{\odot}$	$M_{\text{Projected}}$ $h^{-1} M_{\odot}$	W	N	p
CIZA J1324.7–5736	5570 ± 92	618 ± 72	$(3.5 \pm 1.0) \times 10^{14}$	$(3.9 \pm 0.7) \times 10^{14}$	0.9555	40	0.1176
Abell S0639A	6501 ± 61	405 ± 40	$(1.2 \pm 0.3) \times 10^{14}$	$(1.7 \pm 0.4) \times 10^{14}$	0.983	40	0.7987
Abell S0639B	14125 ± 66	412 ± 39	$(3.6 \pm 0.8) \times 10^{14}$	$(5.3 \pm 0.6) \times 10^{14}$	0.951	41	0.0648
Triangulum Australis (corrected)	15060 ± 97	1408 ± 67	$(5.7 \pm 0.6) \times 10^{15}$	$(6.9 \pm 0.5) \times 10^{15}$	0.9855	220	0.0242
	14898 ± 90	1246 ± 59	$(4.4 \pm 0.4) \times 10^{15}$	$(5.4 \pm 0.4) \times 10^{15}$	0.9919	210	0.2945
Ara	14634 ± 76	881 ± 48	$(2.0 \pm 0.3) \times 10^{15}$	$(2.6 \pm 0.2) \times 10^{15}$	0.9840	147	0.0850
CIZA J1514.6–4558	16715 ± 50	601 ± 35	$(1.2 \pm 0.1) \times 10^{15}$	$(1.5 \pm 0.1) \times 10^{15}$	0.9953	149	0.9145
CIZA J1410.4–4246A	15574 ± 63	497 ± 40	$(5.2 \pm 0.9) \times 10^{14}$	$(6.2 \pm 0.8) \times 10^{14}$	0.9761	66	0.2328
CIZA J1410.4–4246B	20463 ± 53	345 ± 37	$(5.3 \pm 1.3) \times 10^{14}$	$(7.5 \pm 0.8) \times 10^{14}$	0.9569	45	0.0922
Cluster 1 (Field 9)	21445 ± 78	925 ± 52	$(3.1 \pm 0.3) \times 10^{15}$	$(3.8 \pm 0.3) \times 10^{15}$	0.9851	151	0.1023
Cluster 2 (Field 25)	-	-	-	-	0.9685	85	0.0354

Comparison with the Norma cluster velocity dispersion of 897 km s⁻¹ (Kraan-Korteweg et al. 1996) suggests that CIZA J1324.7–5736 is approximately 0.3–0.5 times as massive. This is in agreement with the Mullis et al. (2005) comparison of XMM-Newton observations of CIZA J1324.7–5736 with the X-ray temperature of the Norma cluster inferred by Tamura et al. (1998). Using the mass-temperature scaling relations, they conclude that CIZA J1324.7–5736 contains about a third of the mass of the Norma cluster. A future study of the extinction-corrected K_S -band luminosity function should provide further constraints on the relative mass (Nagayama et al. 2005).

The second distinct feature observed in the fields is that of the Cen-Crux overdensity itself. This appears as a filament like trail of galaxies separated from the X-ray source both spatially on the sky and in redshift. Although no connective structure is evident between this overdensity and CIZA J1324.7–5736, their close proximity suggest that they are gravitationally bound. As the structure is not dynamically relaxed, virial theorem does not apply. However the extent of the Cen-Crux structure and the number of galaxies contained within it implies a mass similar to that of the CIZA J1324.7–5736 cluster.

3.2.2 PKS 1343–601

PKS 1343–601 is the second brightest extragalactic radio source in the southern sky (Mills 1952). The associated galaxy, lying at (309.7°, +1.7°, 3872 km s⁻¹, West & Tarengi 1989), is a large elliptical galaxy (Laustsen et al. 1977; West & Tarengi 1989), typical of those found in cluster cores. Hence it has been suggested that PKS 1343–601 may mark the centre of another highly obscured ($A_B \sim 12$) cluster (Woudt 1998; Kraan-Korteweg & Woudt 1999).

X-ray studies have yet to reveal any indication that such a hidden cluster exists. No corresponding source is seen in the CIZA survey and the point-like X-ray emissions reported by Tashiro et al. (1998) are consistent with the radio lobes of PKS 1343–601 rather than intracluster gas (Ebeling et al. 2002). However in HIPASS observations, a small overdensity around the radio galaxy has been detected (Kraan-Korteweg et al. 2005b). The nature of this overdensity has recently been examined by three near-infrared surveys (Schröder et al. 2005; Kraan-Korteweg et al. 2005a;

Nagayama et al. 2004). Through radial velocity studies, simulated sky-projections and extrapolation of luminosity functions, these surveys are all consistent with the notion of a low mass group or poor cluster centred on PKS 1343–601.

Unfortunately, of the 84 targets we identified in the 2dF field, our 6300 s observation yielded only five reliable redshifts. Of these is a reconfirmation of the redshift of PKS 1343–601. At 4065 ± 85 km s⁻¹, this is in agreement with the West & Tarengi (1989) value. Of the other four new measurements, all identified through emission lines, two are located within 500 km s⁻¹ of the radio galaxy. NWN2004 45 and NWN2004 51 are both taken from the Nagayama et al. (2004) catalogue and lie at 3861 and 3571 km s⁻¹ respectively. These galaxies, together with those identified both optically and in HI by Schröder et al. (2005), brings the number of galaxies with known redshifts that are associated with the PKS 1343–601 group up to 20.

3.2.3 Abell S0639

The Abell S0639 cluster, which lies at (281°, +11°), was first studied in detail by Stein (1994, 1997), who for 32 galaxies measured a mean velocity of 6194 ± 78 km s⁻¹ and a velocity dispersion of 431 ± 52 km s⁻¹. Using a sample of 40 galaxies with a mean $cz = 6501 \pm 61$ km s⁻¹, we find a similar dispersion of 409 ± 55 km s⁻¹. An additional feature is located in the same field, offset from Abell S0639 by 1.5°. At 14065 ± 69 km s⁻¹, the structure lies at the same distance as the SSC and is not inconsistent with a normal distribution (p-value = 0.0648). The measured virial velocity dispersion is 597 ± 91 km s⁻¹, corresponding to a mass of $(4.9 \pm 1.2) \times 10^{14} h^{-1} M_{\odot}$.

3.2.4 Triangulum Australis, Ara, CIZA J1638.2–6420, CIZA J1514.6–4558 & CIZA J1410.4–4246

In the extended CIZA catalogue, Kocevski et al. (2005) have identified several X-ray sources located at $z \sim 0.05$, which they suggest form an extension to the SSC. In Ebeling et al. (2002), the same authors argue that these clusters may be responsible for the observed continued flow towards a point behind the GA. Of these sources we have targeted the four largest: CIZA J1638.2–6420 (the Triangulum-Australis cluster) at (324.5°, –11.6°, 15060 km s⁻¹), CIZA J1653.0–5943 (the Ara cluster, Woudt

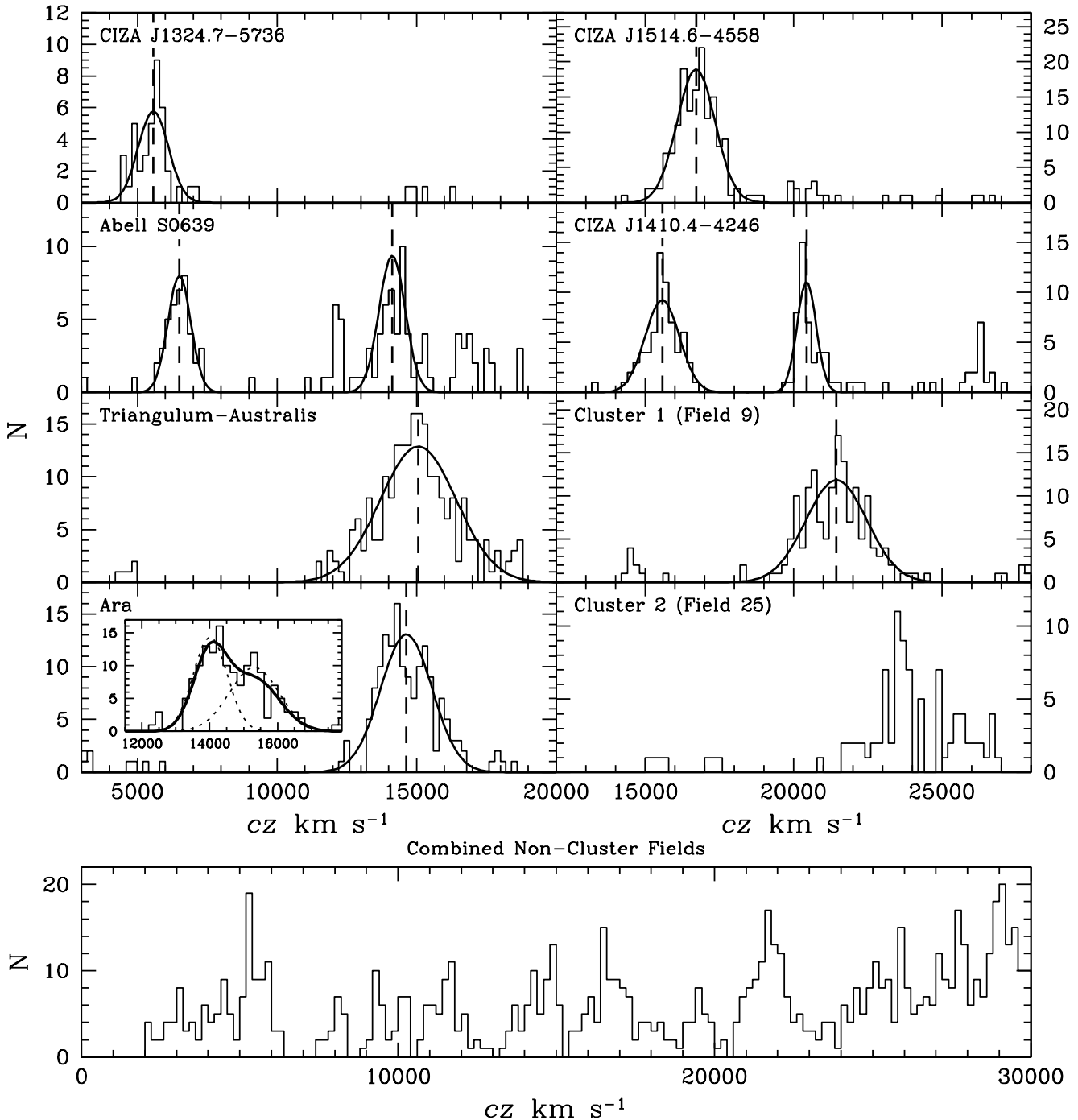


Figure 5. The radial velocity dispersions and corresponding virial fits for the observed clusters are shown in the upper panel. The lower panel shows the combined velocity distribution for the 11 non-cluster fields.

1998) at (329.3° , -9.9° , 14634 km s⁻¹), CIZA J1410.4-4246 (318.0° , 17.8° , 15574 km s⁻¹) and CIZA J1514.6-5736 (327.3° , 10.0° , 16715 km s⁻¹). All four structures have clearly identified Gaussian velocity distributions from which we are able to infer virial and projected masses as listed in table 3. The Triangulum-Australis cluster yields a noticeably low p-value (0.0242). This is due to the overdensity seen in the right hand tail of the dispersion. Remov-

ing the 10 galaxies with $cz > 18000$ km s⁻¹ from the field results in a more respectable p-value of 0.2945 (listed as corrected in table 3). With a corresponding virial mass of $(5.7 \pm 0.6) \times 10^{15} h^{-1} M_\odot$, this large cluster is similar in mass to the Norma cluster.

Despite a p-value of 0.0850, the Ara cluster appears to display a bimodal velocity distribution. Fitting two Gaussian profiles to the data results in velocity disper-

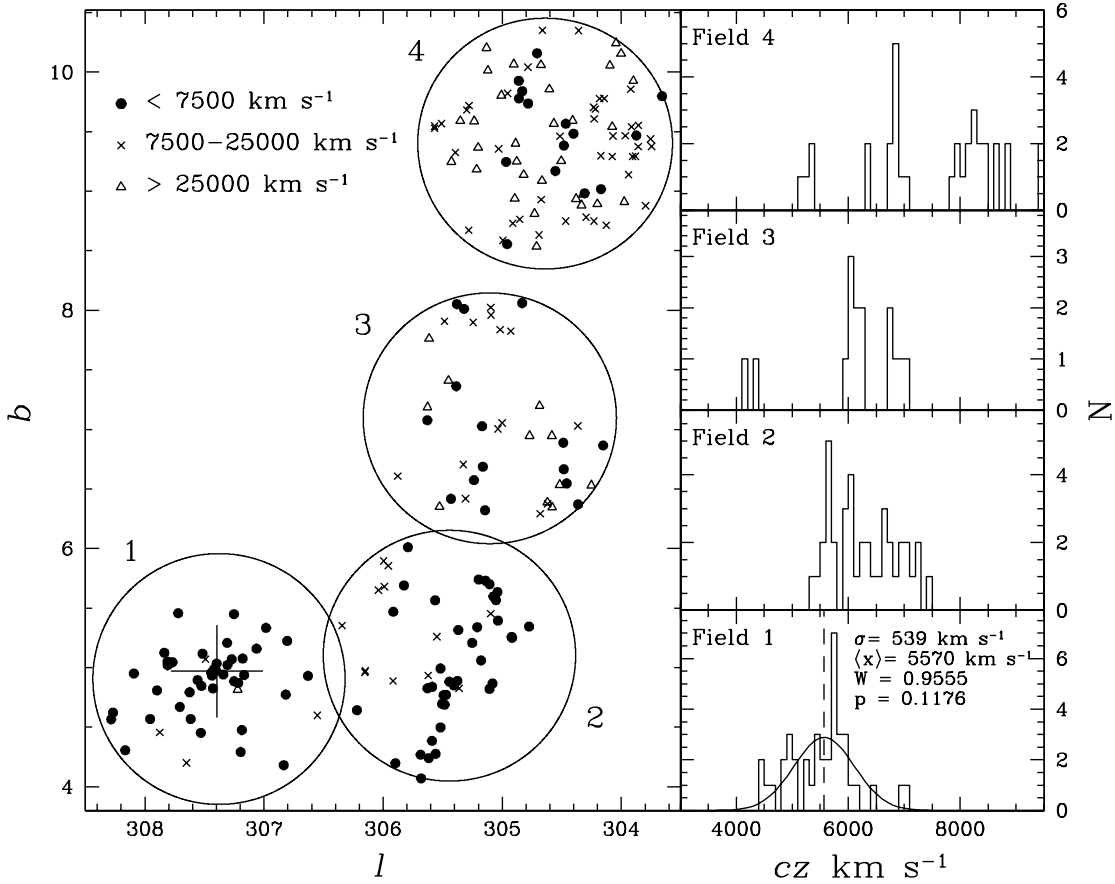


Figure 6. Galactic longitude and latitude of galaxies measured by this survey for the four denoted 2dF fields in the Cen-Crux region. The large cross marks the centre of the X-ray source CIZA J1324.7–5736. The right hand panels show the corresponding velocity histograms for each of the fields between 3000 and 9500 km s^{-1} .

sions of $498 \pm 68 \text{ km s}^{-1}$ and $731 \pm 112 \text{ km s}^{-1}$ centred on $14016 \pm 84 \text{ km s}^{-1}$ and $15310 \pm 124 \text{ km s}^{-1}$ respectively. These fits are shown in the inset to the Ara cluster panel of Fig. 5. There is no discernible separation in the projected sky distribution of the two populations, hence they may be two infalling clumps collapsing along the line of sight. A 7.5 ks *ROSAT* HRI observation of the cluster supports this argument, as two distinct peaks, separated by only 4 arcmin, were observed in the elongated X-ray emissions (Ebeling et al. 2002). Summed in quadrature, the two velocity dispersions are similar to the dispersion of the overall fit ($881 \pm 48 \text{ km s}^{-1}$); hence, even though virial theorem is not strictly applicable to such a system, the mass derived from the total fit provides a likely upper limit to the combined mass of the two clumps.

The results of the Shapiro-Wilk test for CIZA J1514.6–4558 and CIZA J1410.4–4246 indicate that they are consistent with being dynamically relaxed clusters as shown in Fig. 5. Behind CIZA J1410.4–4246 there appears a second group with a velocity dispersion consistent with a normal distribution. However with a skewness of 0.094, the mean distance and the velocity dispersion of the feature are likely overestimated.

The Triangulum-Australis and Ara clusters are physically separated by only $\sim 13.7 h^{-1} \text{ Mpc}$ and lie in ap-

proximately the same plane as the CIZA J1514.6–4558 and CIZA J1410.4–4246 clusters. Abell 3558, the core of the SSC, lies only 38 Mpc from CIZA J1410.4–4246 and so these clusters may well form an extension to the SSC. Nevertheless the presence of such large masses in close proximity to each other has a sizeable influence on the X-ray based dipole (Kocevski et al. 2004). The effects of this will be studied in more detail by a subsequent paper.

3.2.5 Additional Clusters

Examination of 2MASS maps of the GA/SSC region reveals two further overdensities centred on $(314.5^\circ, +13.7^\circ)$ and $(321.7^\circ, +13.4^\circ)$. These were targeted in fields 9 ($314.3^\circ, +13.9^\circ$) and 25 ($322.3^\circ, +13.6^\circ$) respectively. Recently, Kocevski et al. (2005) have reported the presence of an X-ray source, identified as CIZA J1358.7–4750, at $(314.5^\circ, +13.5^\circ)$, coincident with the structure in field 9. At $cz = 21445 \pm 78 \text{ km s}^{-1}$ this cluster is far enough removed to have little influence ($V_{\text{LG}} < 3 \text{ km s}^{-1}$) on local dynamics despite the large predicted mass ($\sim 3 \times 10^{15} h^{-1} M_\odot$).

As evident in the lower right panel of Fig. 5, The galaxies between 21000 and 27000 km s^{-1} in field 25 are concentrated into numerous sub-clumps loosely associated in a broad distribution. The associated p-value of 0.0345 con-

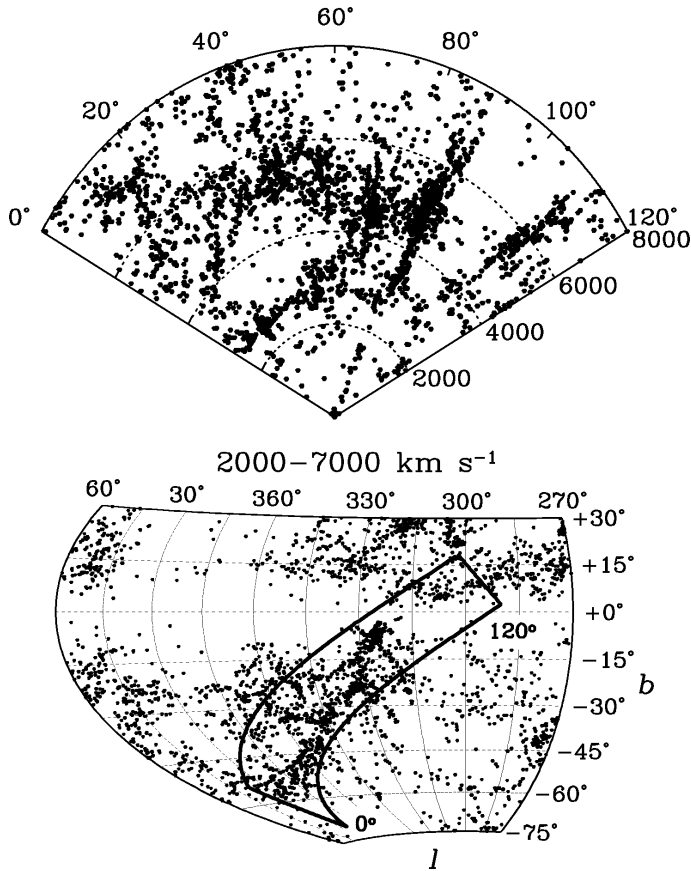


Figure 7. The pieplot represents the radial distribution of galaxies along the projected rectangular strip shown in the lower panel. The strip covers a region $120^\circ \times 10^\circ$, orientated to lie along the filament. From the Norma cluster, lying 86° along the strip, the Norma supercluster is clearly seen as a wall of galaxies extending through the Pavo II cluster (at 71°) towards a point $\sim 20^\circ$ along the strip. The Centaurus Wall appears as a smaller connection of galaxies, running almost parallel to the Norma supercluster at 2600 km s^{-1} . The void lying between the Norma supercluster and the Centaurus Wall is an extension of the massive Microscopium Void.

firms that this is not consistent with a dynamically relaxed cluster and hence we do not assign it a mass.

3.3 The Extended Norma Supercluster

Several large clusters are now known to reside in the GA region, i.e. Norma, Pavo II, Centaurus, Hydra and CIZA J1324.7–5736. However the connections between these clusters are still poorly resolved. As shown in Fig. 4, the Pavo II and Norma clusters are connected by a structure, which Woudt et al. (1997) have suggested extends through the ZoA towards the Cen-Crux overdensity. This connection is highlighted by the noticeable peak around 5500 km s^{-1} in the combined velocity distribution of non-cluster fields shown in the bottom panel of Fig. 5. To examine this feature further, Fig. 7 and Fig. 8 plot redshift slices of the filament below and above the Galactic plane.

Evident in the foreground of the diagram in the upper panel of Fig. 7 is the Centaurus Wall. Appearing as a fila-

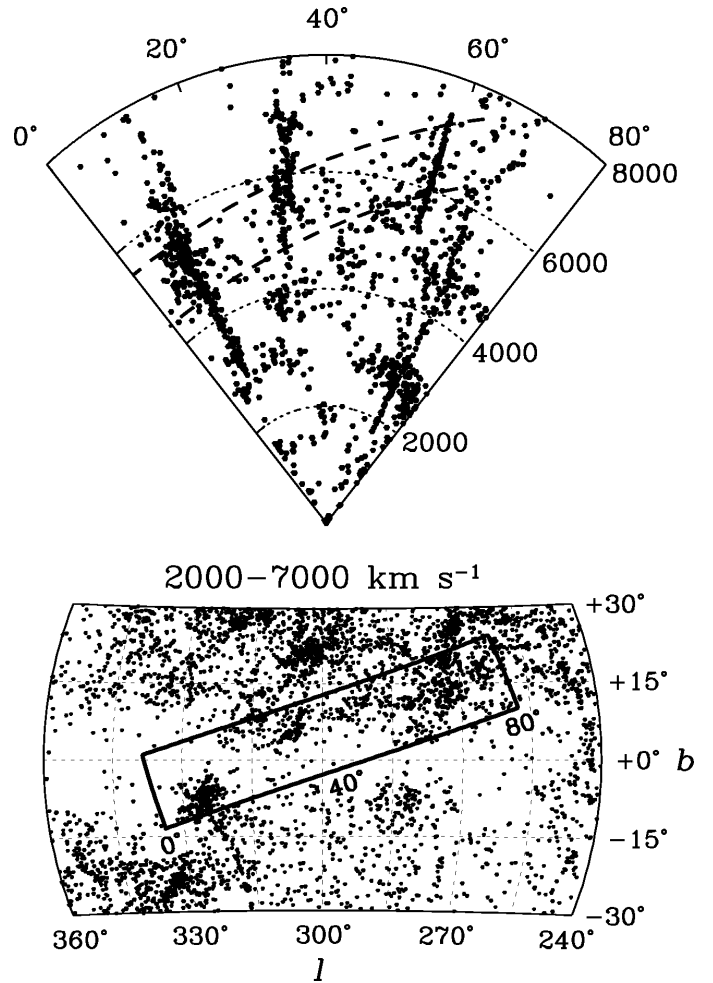


Figure 8. The pieplot contains the galaxies in the $80^\circ \times 15^\circ$ rectangular strip shown in the Aitoff projection. The proposed Norma supercluster, seen as a trail of galaxies lying between the dashed lines, connects the ‘fingers-of-God’ of the Norma cluster (11° , 4500 km s^{-1}), CIZA J1324.7–5736 (31° , 5570 km s^{-1}) and Abell S0639 (58° , 6501 km s^{-1}). The overdensity at (70° , 2800 km s^{-1}) is the superposition of the Antlia cluster and the Hydra-Antlia extension seen in cross-section.

ment of galaxies running across the sky at $cz \sim 2600 \text{ km s}^{-1}$, this structure is separated by some 2000 km s^{-1} from the Norma structure. This is in contradiction with earlier studies that have suggested the Norma cluster is a nexus between the Centaurus Wall and the Norma Supercluster (Woudt et al. 1997). The dearth of galaxies in the ZoA is clearly seen as the gap in the wall between the Norma and CIZA J1324.7–5736 clusters, which respectively appear as ‘fingers-of-God’ at 86° and 108° along the strip. However, below the ZoA, the extent of the structure is clearly evident as the broad wall of galaxies extends out from the Norma cluster, through the Pavo II cluster and on towards higher redshifts. In the Aitoff projection shown in the lower panel of Fig. 7, many additional, smaller filaments are seen branching off from the main structure, primarily at the location of the clusters. However a major branch splits off at around $\sim (345^\circ, -35^\circ, 5000 \text{ km s}^{-1})$ and continues to $\sim (17^\circ, -22^\circ, 6000 \text{ km s}^{-1})$. The main filament appears to disperse

at $\sim (5^\circ, -50^\circ, 5000 \text{ km s}^{-1})$, with apparent overdensities at greater galactic longitudes ($5^\circ < l < 30^\circ$, $-60^\circ < b < -45^\circ$) resulting from the projection along the line of sight of clumps, including galaxies in the Centaurus Wall.

Fig. 8 shows a possible extension of the Norma supercluster filament through the plane to higher galactic latitudes. Here the progression to higher redshifts is hinted at as the filament extends from the Norma Cluster (lying 11° along the strip), through CIZA J1324.7–5736 (at 31°) and the Cen-Crux feature (33°) and on towards Abell S0639 (58°). From this last cluster an extension towards another overdensity located off the panel at (268° , $+17^\circ$, 9000 km s^{-1}) may exist, but lack of redshifts makes this difficult to discern. The Vela overdensity (280° , $+6^\circ$, 6000 km s^{-1}) lies next to Abell S0639 and so forms a spur to the main filament. However, another intercluster connection from Abell S0639 appears to run at almost right angles to the Norma supercluster. This filament extends through the overdensity located at (272° , $+13^\circ$, 4500 km s^{-1}), which is likely associated with Abell S0631 and Abell S0628, both of which currently have no reported redshift, before joining the Hydra cluster. As detailed in Section 3.1, the large Hydra cluster is connected by the Hydra Wall to the Centaurus cluster and by the Hydra-Antlia extension to the Antlia cluster and galaxies at lower galactic latitudes.

Thus, from Abell S0639 to $\sim (5^\circ, -50^\circ)$, there appears to exist a continuous filament of galaxies stretching across approximately 100° (i.e. $\sim 120 \text{ Mpc}$) of the southern sky, with a velocity dispersion $< 400 \text{ km s}^{-1}$. From studies of inter-cluster filaments in simulations, Colberg, Krughoff & Connolly (2005) find a typical overdensity along these structures of ~ 7 and cross-sectional radii of $\sim 2 h^{-1} \text{ Mpc}$. Thus, not including the associated clusters, a filament of this size, dynamically centred at $\sim (325^\circ, -10^\circ, 4800 \text{ km s}^{-1})$, might contain a mass as high as $\sim 2.5 \times 10^{15} h^{-1} M_\odot$. This is comparable to the mass of a large cluster and so represents another potentially significant component of the GA.

4 SUMMARY

Using the 2dF on the AAT, we have measured 3053 redshifts in the GA/SSC region, of which 2603 are new measurements. These redshifts have helped reveal the composition of the GA, principally with the resolution of the CIZA J1324.7–5736/Cen-Crux feature. The X-ray source is revealed to be a dynamically relaxed cluster with a mass approximately 0.3–0.5 times that of the Norma Cluster, in good agreement with previous estimates.

By combining the results of this survey with redshifts from the literature, the major clusters associated with the GA are found to be joined by a possibly wall-like structure. This filament extends from Abell S0639, through the ZOA, where it meets the Norma cluster, and continues down to $\sim (5^\circ, -50^\circ, 5000 \text{ km s}^{-1})$. Together with the Norma, Pavo II, CIZA J1324.7–5736 and Abell S0639 clusters, we can expect these structures to contribute a mass of $\sim 10^{16} h^{-1} M_\odot$ towards the GA.

We have also measured the masses and composition of several other clusters behind the GA, including the Triangulum-Australis, Ara, CIZA J1514.6–4558 and

CIZA J1410.4–4246 clusters. These have been proposed as possible sources to a continued flow beyond the GA. The results from all these observations will be used in a subsequent paper to model the flows in this complex and important region.

5 ACKNOWLEDGEMENTS

This paper is based on research taken with the 2dF at the AAT telescope. We wish to thank all the AAO staff, in particular Scott Croom and Rob Sharp, for their help and continued support of 2dF. DJR-S thanks PPARC for a research studentship. This research has also made use of the NASA/IPAC Extragalactic Database (NED) which is operated by the Jet Propulsion Laboratory, California Institute of Technology, under contract with the National Aeronautics and Space Administration and data products from 2MASS, which is a joint project of the University of Massachusetts and the Infrared Processing and Analysis Center/California Institute of Technology, funded by the National Aeronautics and Space Administration and the National Science Foundation.

REFERENCES

- Aaronson M., et al., 1989, *ApJ*, 338, 654
- Bardelli S., Zucca E., Zamorani G., Moscardini L., Scaramella R., 2000, *MNRAS*, 312, 540
- Barnes D. G., et al., 2001, *MNRAS*, 322, 486
- Branchini E., et al., 1999, *MNRAS*, 308, 1
- Cappi A., et al., 1998, *A&A*, 336, 445
- Colberg J. M., Krughoff K. S., Connolly A. J., 2005, *MNRAS*, 359, 272
- Cole S., et al., 2001, *MNRAS*, 326, 255
- Colless M., et al., 2001, *MNRAS*, 328, 1039
- Cutri R. M., et al., 2003, *VizieR Online Data Catalog*, 2246
- Danese L., de Zotti G., di Tullio G., 1980, *A&A*, 82, 322
- Ebeling H., Mullis C. R., Tully R. B., 2002, *ApJ*, 580, 774
- Ettori S., Fabian A. C., White D. A., 1997, *MNRAS*, 289, 787
- Faber S. M., Burstein D., 1988, *Motions of galaxies in the neighborhood of the local group. Large-Scale Motions in the Universe: A Vatican study Week*, pp 115–167
- Fairall A. P., ed. 1998
- Fairall A. P., Woudt P. A., Kraan-Korteweg R. C., 1998, *A&ASS*, 127, 463
- Hasegawa T., et al., 2000, *MNRAS*, 316, 326
- Heisler J., Tremaine S., Bahcall J. N., 1985, *ApJ*, 298, 8
- Henning P. A., Kraan-Korteweg R. C., Stavely-Smith L., 2005, in *ASP Conf. Ser. 329: Nearby Large-Scale Structures and the Zone of Avoidance* p. 199
- Høg E., Fabricius C., Makarov V. V., Urban S., Corbin T., Wycoff G., Bastian U., Schwekendiek P., Wicenec A., 2000, *A&A*, 355, 27
- Huchra J. P., Geller M. J., Clemens C. M., Tokarz S. P., Michel A., 1992, *Bull. CDS*, 41, 31
- Hudson M. J., 1994, *MNRAS*, 266, 468
- Hudson M. J., Smith R. J., Lucey J. R., Branchini E., 2004, *MNRAS*, 352, 61

- Jarrett T. H., Chester T., Cutri R., Schneider S., Skrutskie M., Huchra J. P., 2000, *AJ*, 119, 2498
- Jones D. H., Saunders W., Read M., Colless M., 2005, *PASA*, 22, 277
- Kaldare R., Colless M., Raychaudhury S., Peterson B. A., 2003, *MNRAS*, 339, 652
- Kocevski D. D., Ebeling H., Mullis C. R., Tully R. B., 2005, *ArXiv:astro-ph/0512321*
- Kocevski D. D., Mullis C. R., Ebeling H., 2004, *ApJ*, 608, 721
- Kolatt T., Dekel A., Lahav O., 1995, *MNRAS*, 275, 797
- Koribalski B. S., 2005, in *ASP Conf. Ser. 329: Nearby Large-Scale Structures and the Zone of Avoidance* p. 217
- Koribalski B. S., et al., 2004, *AJ*, 128, 16
- Kraan-Korteweg R. C., Fairall A. P., Balkowski C., 1995, *A&A*, 297, 617
- Kraan-Korteweg R. C., Ochoa M., Woudt P. A., Andernach H., 2005a, in *Fairall A. P., Woudt P. A., eds, ASP Conf. Ser. Vol. 329, Nearby Large-Scale Structures and the Zone of Avoidance. Astron. Soc. Pac., San Francisco*, pp 159–165
- Kraan-Korteweg R. C., Staveley-Smith L., Donley J., Koribalski B., Henning P. A., 2005b, in *Colless M., Staveley S., Stathakis R., eds, ASP Conf. Ser. Vol. 216, Maps of the Cosmos* pp 203–210
- Kraan-Korteweg R. C., Woudt P. A., 1994, in *ASP Conf. Ser. 67: Unveiling Large-Scale Structures Behind the Milky Way* p. 89
- Kraan-Korteweg R. C., Woudt P. A., 1999, *PASA*, 16, 53
- Kraan-Korteweg R. C., Woudt P. A., Cayatte V., Fairall A. P., Balkowski C., Henning P. A., 1996, *Nat*, 379, 519
- Lahav O., Yamada T., Scharf C., Kraan-Korteweg R. C., 1993, *MNRAS*, 262, 711
- Laustsen S., Schuster H.-E., West R. M., 1977, *A&A*, 59, 3
- Lucey J., Radburn-Smith D., Hudson M., 2005, in *ASP Conf. Ser. 329: Nearby Large-Scale Structures and the Zone of Avoidance* p. 21
- Lucey J. R., Carter D., 1988, *MNRAS*, 235, 1177
- Lynden-Bell D., Faber S. M., Burstein D., Davies R. L., Dressler A., Terlevich R. J., Wegner G., 1988, *ApJ*, 326, 19
- Mathewson D. S., Ford V. L., Buchhorn M., 1992, *ApJL*, 389, 5
- Meyer M. J., et al., 2004, *MNRAS*, 350, 1195
- Mills B. Y., 1952, *Australian J. Sci. Res. serie A* 5, 5, 266–287 (1952), 5, 266
- Mullis C. R., Ebeling H., Kocevski D. D., Tully R. B., 2005, in *ASP Conf. Ser. 329: Nearby Large-Scale Structures and the Zone of Avoidance* p. 183
- Nagayama T., et al., 2004, *MNRAS*, 354, 980
- Nagayama T., Nagata T., Sato S., Woudt P. A., Irsf/Sirius Team 2005, in *ASP Conf. Ser. 329: Nearby Large-Scale Structures and the Zone of Avoidance* p. 177
- Proust D., et al., 2005, *arXiv:astro-ph/0509903*
- Raychaudhury S., 1989, *Nat*, 342, 251
- Reisenegger A., Quintana H., Carrasco E. R., Maze J., 2000, *AJ*, 120, 523
- Rines K., Geller M. J., Kurtz M. J., Diaferio A., 2003, *AJ*, 126, 2152
- Rowan-Robinson M., et al., 2000, *MNRAS*, 314, 375
- Royston P., 1995, *Applied Statistics*, 44, 547
- Scaramella R., Baiesi-Pillastrini G., Chincarini G., Vettolani G., Zamorani G., 1989, *Nature*, 338, 562
- Schröder A. C., Kraan-Korteweg R. C., Mamon G. A., Woudt P. A., 2005, in *Fairall A. P., Woudt P. A., eds, ASP Conf. Ser. Vol. 329, Nearby Large-Scale Structures and the Zone of Avoidance. Astron. Soc. Pac., San Francisco*, pp 167–176
- Shapiro S. S., Wilk M. B., 1965, *Biometrika*, 52, 591
- Smith R. J., Hudson M. J., Lucey J. R., Schlegel D. J., Davies R. L., 2000, in *Astronomical Society of the Pacific Conference Series* p. 39
- Stein P., 1994, Ph.D. thesis, University of Basel
- Stein P., 1996, *A&ASS*, 116, 203
- Stein P., 1997, *A&A*, 317, 670
- Tamura T., Fukazawa Y., Kaneda H., Makishima K., Tashiro M., Tanaka Y., Bohringer H., 1998, *PASJ*, 50, 195
- Tashiro M., et al., 1998, *ApJ*, 499, 713
- Tonry J., Davis M., 1979, *AJ*, 84, 1511
- Tonry J. L., Blakeslee J. P., Ajhar E. A., Dressler A., 2000, *ApJ*, 530, 625
- Wakamatsu K., Malkan M. A., Nishida M. T., Parker Q. A., Saunders W., Watson F. G., 2005, in *Fairall A. P., Woudt P. A., eds, ASP Conf. Ser. Vol. 329, Nearby Large-Scale Structures and the Zone of Avoidance. Astron. Soc. Pac., San Francisco*, pp 189–198
- West R. M., Tarengi M., 1989, *A&A*, 223, 61
- Woudt P. A., 1998, Ph.D. thesis, University of Cape Town
- Woudt P. A., Fairall A. P., Kraan-Korteweg R. C., 1997, in *ASP Conf. Ser. Vol. 117, Dark and Visible Matter in Galaxies and Cosmological Implications* pp 373–379
- Woudt P. A., Kraan-Korteweg R. C., Cayatte V., Balkowski C., Felenbok P., 2004, *A&A*, 415, 9
- Woudt P. A., Kraan-Korteweg R. C., Fairall A. P., 1999, *A&A*, 352, 39